



HAL
open science

Determining Effective Temporal Windows for Rapeseed Detection Using Sentinel-1 Time Series and Machine Learning Algorithms

Saeideh Maleki, Nicolas Baghdadi, Sami Najem, Cassio Fraga Dantas, Hassan Bazzi, Dino Ienco

► To cite this version:

Saeideh Maleki, Nicolas Baghdadi, Sami Najem, Cassio Fraga Dantas, Hassan Bazzi, et al.. Determining Effective Temporal Windows for Rapeseed Detection Using Sentinel-1 Time Series and Machine Learning Algorithms. *Remote Sensing*, 2024, 16 (3), pp.549. 10.3390/rs16030549 . hal-04476131

HAL Id: hal-04476131

<https://hal.science/hal-04476131>

Submitted on 4 Mar 2024

HAL is a multi-disciplinary open access archive for the deposit and dissemination of scientific research documents, whether they are published or not. The documents may come from teaching and research institutions in France or abroad, or from public or private research centers.

L'archive ouverte pluridisciplinaire **HAL**, est destinée au dépôt et à la diffusion de documents scientifiques de niveau recherche, publiés ou non, émanant des établissements d'enseignement et de recherche français ou étrangers, des laboratoires publics ou privés.



Distributed under a Creative Commons Attribution 4.0 International License



Article

Determining Effective Temporal Windows for Rapeseed Detection Using Sentinel-1 Time Series and Machine Learning Algorithms

Saeideh Maleki ¹, Nicolas Baghdadi ¹ , Sami Najem ¹, Cassio Fraga Dantas ¹ , Hassan Bazzi ² and Dino Ienco ^{1,*}

¹ TETIS, Université de Montpellier, INRAE, CIRAD, CNRS, 34093 Montpellier, France; saeideh.maleki-najafabadi@inrae.fr (S.M.); nicolas.baghdadi@inrae.fr (N.B.); sami.najem@inrae.fr (S.N.); cassio.fraga-dantas@inrae.fr (C.F.D.)

² Atos France, Technical Services, 80 Quai Voltaire, 95870 Bezons, France; hassan.bazzi@atos.net

* Correspondence: dino.ienco@inrae.fr

Abstract: This study investigates the potential of Sentinel-1 (S1) multi-temporal data for the early-season mapping of the rapeseed crop. Additionally, we explore the effectiveness of limiting the portion of a considered time series to map rapeseed fields. To this end, we conducted a quantitative analysis to assess several temporal windows (periods) spanning different phases of the rapeseed phenological cycle in the following two scenarios relating to the availability or constraints of providing ground samples for different years: (i) involving the same year for both training and the test, assuming the availability of ground samples for each year; and (ii) evaluating the temporal transferability of the classifier, considering the constraints of ground sampling. We employed two different classification methods that are renowned for their high performance in land cover mapping: the widely adopted random forest (RF) approach and a deep learning-based convolutional neural network, specifically the InceptionTime algorithm. To assess the classification outcomes, four evaluation metrics (recall, precision, F1 score, and Kappa) were employed. Using S1 time series data covering the entire rapeseed growth cycle, the tested algorithms achieved F1 scores close to 95% on same-year training and testing, and 92.0% when different years were used, both algorithms demonstrated robust performance. For early rapeseed detection within a two-month window post-sowing, RF and InceptionTime achieved F1 scores of 67.5% and 77.2%, respectively, and 79.8% and 88.9% when extended to six months. However, in the context of temporal transferability, both classifiers exhibited mean F1 scores below 50%. Notably, a 5-month time series, covering key growth stages such as stem elongation, inflorescence emergence, and fruit development, yielded a mean F1 score close to 95% for both algorithms when trained and tested in the same year. In the temporal transferability scenario, RF and InceptionTime achieved mean F1 scores of 92.0% and 90.0%, respectively, using a 5-month time series. Our findings underscore the importance of a concise S1 time series for effective rapeseed mapping, offering advantages in data storage and processing time. Overall, the study establishes the robustness of RF and InceptionTime in rapeseed detection scenarios, providing valuable insights for agricultural applications.

Keywords: rapeseed mapping; Sentinel-1; machine learning; neural networks



Citation: Maleki, S.; Baghdadi, N.; Najem, S.; Dantas, C.F.; Bazzi, H.; Ienco, D. Determining Effective Temporal Windows for Rapeseed Detection Using Sentinel-1 Time Series and Machine Learning Algorithms. *Remote Sens.* **2024**, *16*, 549. <https://doi.org/10.3390/rs16030549>

Academic Editor: Peng Fu

Received: 16 December 2023

Revised: 23 January 2024

Accepted: 24 January 2024

Published: 31 January 2024



Copyright: © 2024 by the authors. Licensee MDPI, Basel, Switzerland. This article is an open access article distributed under the terms and conditions of the Creative Commons Attribution (CC BY) license (<https://creativecommons.org/licenses/by/4.0/>).

1. Introduction

The growing demands for vegetable oil and biofuel have led to the expansion of rapeseed cultivation [1]. Consequently, the provision of precise and timely information on rapeseed cultivation is crucial for agricultural policies [2]. The accuracy of this information can be influenced by various factors, such as the diversity among producers, agricultural management strategies, soil conditions, and climate [1,3]. Recognizing and utilizing diverse tools that aid in rapeseed detection is vital to alleviating the impact of these diverse factors.

Incorporating advanced technologies and remote sensing methods notably enhances the accuracy of rapeseed crop data. Ultimately, this advancement will foster more resilient and effective agricultural management strategies.

Remote sensing data acquired at various spatial, spectral, and temporal resolutions have become paramount sources of information for monitoring the cultivation of crops. Such information can, nowadays, be used as an input for modern machine learning and deep learning algorithms to enhance agricultural monitoring, as in the case of rapeseed mapping [4,5]. Tao et al. [6] achieved 92% accuracy in creating a rapeseed map utilizing the Landsat images. They employed an artificial neural network (ANN)-based method to map winter rapeseed. Zhang et al. [1] used the 2DCNN algorithm to detect rapeseed, achieving an accuracy of 0.91. Their study focused on classifying images from five different optical satellites (GF-1, S2, L7, L8, and GF-6). However, the performance of various deep learning and machine learning algorithms appears to be influenced by factors such as the size of the training dataset. Maleki et al. [7] conducted an evaluation on the impact of training sample size on the performance of three deep learning and one machine learning algorithm for rapeseed mapping. They demonstrated that using sample sizes ranging from 300 to 1000, random forest (RF) and InceptionTime exhibited higher accuracy (F1 score > 90%) compared to the long short-term memory fully convolutional network (LSTM-FCN) and multi-layer perceptron (MLP). Previous studies have shown high accuracy in rapeseed detection using a time series analysis, overcoming challenges faced by single-image methods in regions with complex crop cultivation [3,5,8–13]. For instance, Mercier et al. [11] reported an accuracy range of 0.74 to 0.92 in rapeseed detection using time series data from Sentinel-1 (S1) and Sentinel 2 (S2). Han et al. [14] achieved F1 scores ranging from 0.92 to 0.95 by integrating time series from Landsat 8 and Sentinel-1 satellite data for rapeseed detection. Waldhoff et al. [15] achieved an F1 score of 86.2% by employing time series data from ASTER, Landsat-5–8, IRS-P6, SPOT-6/7, and RapidEye satellites in their classification process. However, when time series information is considered, determining the effective temporal window (period) for rapeseed classification and using shorter time series data offer advantages in data storage and processing efficiency [2]. Inglada et al. [16] achieved comparable accuracy with both a large multispectral time series and a short time series focusing on the main growth phases of crops. Zhang et al. [1] emphasized the importance of the peak of the crop growth period in the classification of different crops. In addition, the early detection of rapeseed before the end of the cultivation year holds significant value for decision-making, especially in irrigation management and yield forecasting [16,17]. Hence, determining the optimal size of the time series for early rapeseed detection could be useful in providing valuable information to various stakeholders. Vaudour et al. [18] achieved a producer accuracy exceeding 70% using Spot-4 images for rapeseed early detection. Meng et al. [2] proposed an enhancement of wheat and rapeseed mapping by utilizing the Sentinel-2 time series to cover the middle and later stages of the growth cycle. While optical data remain a common choice for early rapeseed detection due to their better understanding of multispectral images and vegetation phenology [16], challenges arise in the winter growth period for rapeseed crops due to frequent and extensive cloud phenomena [4]. The all-weather acquisition capability of synthetic aperture radar (SAR) data makes them valuable for rapeseed detection. For this reason, in this study, arguments related to the time series size and early rapeseed detection are investigated using the time series of S1 images.

This study aims to explore the effective temporal window of the Sentinel-1 (S1) time series for rapeseed detection, emphasizing early detection and the potential use of a short time series. Recent results have shown that deep learning methods exhibit high-level classification performances compared to standard machine learning techniques [19]. Deep learning methods establish mathematical relationships between remote sensing data and crop type information; therefore, they are not dependent on the flowering period of rapeseed [1]. However, this paper will address the question of whether machine learning and deep learning algorithms can effectively detect rapeseed using a limited SAR time series. This research will evaluate different temporal windows (time periods), corresponding to

different rapeseed growth stages, for an accurate mapping of rapeseed in the following two scenarios: (i) involving the same year for both training and testing, and (ii) evaluating the temporal transferability of the classifier (where the training and test data come from different years). In order to classify the S1 time series images, the widely adopted random forest (RF) classifier and a deep learning-based network based on temporal (one-dimensional) convolutions, namely the InceptionTime method, will be employed. The classifier choice is based on previous related studies [7,20], where the chosen strategies have already demonstrated themselves to be robust and well suited for the crop type mapping task.

2. Materials and Methods

2.1. Study Site

The study area is La Rochelle, covering 8000 km² within the Charente-Maritime department in western France (Figure 1). France is the largest contributor to European rapeseed production, accounting for 21% of the European Union's rapeseed production. Notably, the European Union is the world's leading rapeseed producer, accounting for 24% of world production [21]. The main crops cultivated in La Rochelle in 2020 include wheat (27.8%), maize (12.4%), sunflower (9.0%), winter rapeseed (6.0%), and peas (2.4%) (RPG, Registre Parcellaire Graphique). In La Rochelle, rapeseed cultivation usually commences in September and ends in July of the following year [21].

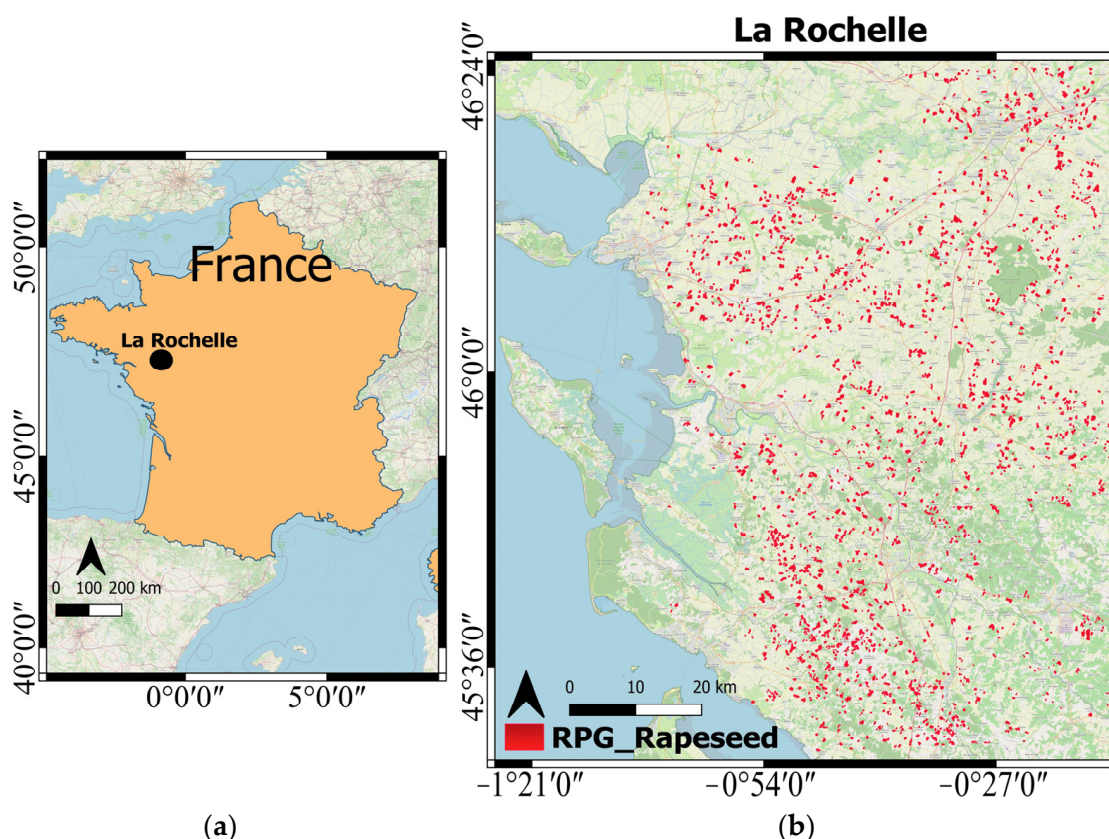


Figure 1. (a) Location of our study site (La Rochelle, France). (b) Rapeseed fields in La Rochelle in 2020.

2.2. Data

2.2.1. Ground Data

We extracted the ground data from the RPG data (French graphical parcel registry), which serves as a database containing farmers' declarations of agricultural fields across the country. This database delineates the boundaries of each declared agricultural field and provides crucial

details, such as crop types and field sizes. Access to the RPG database for all of France is available for download via (<https://www.data.gouv.fr/en/datasets/registre-parcellaire-graphique-rpg-contours-des-parcelles-et-ilots-cultureaux-et-leur-groupe-de-cultures-majoritaire/> (accessed on 20 November 2022)).

2.2.2. SAR Image

We used C-band (5.405 GHz) synthetic aperture radar (SAR) images obtained from the Sentinel-1A (S1A) and Sentinel-1B (S1B) satellites. These images encompassed both “ascending” and “descending” acquisitions, featuring VV and VH polarizations. Each pixel within the S1 images has a spatial resolution of 10 m by 10 m. The revisit schedule of the S1 constellation entails a 6-day cycle when the images of both satellites (S1A and S1B) are employed. For our study site in France, we had access to images from both satellites from three acquisition orbits. These SAR data resources are readily accessible through the European Space Agency’s (ESA) website (<https://scihub.copernicus.eu/dhus/#/home> (accessed on 20 November 2022)). We compiled a dataset comprising images from the three orbits. Regardless of their specific orbit acquisition, all acquired images were arranged in chronological order. Table 1 provides a summary of the total number of S1 images collected at the study site.

Table 1. Sentinel-1 dataset used in this study.

| Study Site | Year | Number of Agricultural Fields | Number of Rapeseed Fields | Number of S1 Images | | | | |
|----------------------|------|-------------------------------|---------------------------|---------------------|----------|----------|----------|----------|
| | | | | Window 1 | Window 2 | Window 3 | Window 4 | Window 5 |
| La Rochelle (France) | 2018 | 77,649 | 2639 | 31 | 90 | 121 | 167 | 77 |
| | 2019 | 71,485 | 1021 | 30 | 86 | 110 | 150 | 64 |
| | 2020 | 96,452 | 1519 | 29 | 88 | 118 | 164 | 76 |

The S1 images were calibrated using the ESA-developed S1 toolbox. The calibration process consists of two main steps: first, radiometric calibration, which converts digital numbers into a backscatter coefficient, σ_0 , in a linear unit; second, geometric correction, which involves orthorectification with a 30 m resolution digital elevation model from the Shuttle Radar Topography Mission (SRTM). Since the analysis was performed on the field scale, the average S1 signal was calculated for each field and for each available S1 image. The aim of this calculation was to obtain a single representative value for each field, thus reducing the speckle effect. In addition, an internal buffer of -10 m (one pixel) was applied along the field boundaries, excluding border pixels from the mean calculation. S1 time series for each rapeseed cultivation year (2018, 2019, and 2020) were created.

2.3. Methodology

In this work, we investigated the likelihood, based on Sentinel-1 (S1) remote sensing data, of accurately detecting rapeseed before the end of the phenological cycle. We also assessed the classification performance using specific, limited periods of the S1 time series. We conducted tests across a variety of temporal windows, reducing the computational burden in the downstream analysis. This not only, in theory, limits data storage, but it also streamlines data download and reduces processing times. The selection of these temporal windows was based on the critical phenological stages of rapeseed in La Rochelle, as documented in the work of Maleki et al. [1].

- Window 1 (W1): Encompasses the leaf production phase of rapeseed (1 September–1 November), with an S1 time series starting at sowing and ending two months later.
- Window 2 (W2): Encompasses both the leaf production phase of rapeseed and its low-rate growth stage during winter (1 September–1 March), with an S1 time series starting at sowing and ending six months later.

- Window 3 (W3): Spans from the beginning of the rapeseed growth cycle until the onset of rapid spring growth (1 September–1 May), with an S1 time series starting at sowing and ending eight months later.
- Window 4 (W4): Encompasses the entire growth stage of rapeseed (1 September–1 August), with an S1 time series starting at sowing and ending eleven months later, just after the harvest.
- Window 5 (W5): Encompasses the crucial stages of rapeseed growth, covering stem elongation, inflorescence emergence, and fruit development (1 March–1 August). Within this temporal window, the S1 time series begins 1–2 months before flowering and ends shortly after harvest. Notably, there is a significant peak in S1 backscatter observed between May and June within this window.

For the classification stage, we adopted RF and InceptionTime algorithms; both methods are renowned for their good performance, as noted in a previous rapeseed mapping study by Maleki et al. [7]. The RF algorithm is an ensemble learning method that combines the outcomes of multiple decision trees to enhance accuracy and prevent overfitting [22]. In this study, 100 trees were used, and default settings were applied for other parameters. InceptionTime, developed by Fawaz et al. [23], is a multivariate time series classification algorithm composed of five convolutional deep learning models, each featuring two residual blocks containing three inception modules [23]. In the training process for the InceptionTime model, the Adam optimizer was employed with fixed parameters ($\beta_1 = 0.9$, $\beta_2 = 0.999$, $\epsilon = 1 \times 10^{-7}$), a learning rate of 1×10^{-5} , and weight decay of 1×10^{-6} . The batch size was set at 16, and a standard cross-entropy loss function was utilized. The classifiers' code utilized in this study using Python 3.8 is available on GitHub (https://github.com/cassiofragadantas/Colza_Classif (accessed on 20 August 2023)). It is important to highlight that in this study, standard parameter settings were employed for the algorithms. This approach ensures a consistent benchmark for evaluating algorithmic performance across various scenarios.

The input data to the classifiers consisted of a time series of VV and VH polarizations, both originating from S1 data, at the field scale (average of backscatter coefficients per field). The classification process focused on identifying rapeseed fields and distinguishing between two classes: rapeseed and non-rapeseed (encompassing all other crop types). We considered two different scenarios: (i) training and test data from the same year, and (ii) training and test data from different years.

Regarding the first scenario, the classification was performed considering all the five temporal windows (W1, W2, W3, W4, and W5). For each year (2018, 2019, and 2020), the data were randomly split into two partitions with a proportion of 70% and 30% for the training and test data, respectively. The procedure was repeated five times to finally average the classification performances in order to avoid possible biases due to the random split procedure.

For the second scenario, the training and test data were taken from different years in order to assess the temporal transferability of the evaluated classifiers. Three temporal windows were used to evaluate this scenario: one for the early detection of rapeseed (among W1/W2/W3), the window covering the entire S1 time series (W4), and finally, the window corresponding to a short S1 time series focused on the main peak of the rapeseed growth cycle (W5). The choice between W1, W2, and W3 depends on the results obtained in the previous scenario. In particular, the chosen window has the ability to provide satisfactory accuracy while using a short period after the sowing date. Temporal transferability of the classifiers was conducted under six combinations of years of training and testing (2018–2019, 2018–2020, 2019–2018, 2019–2020, 2020–2018, and 2020–2019, the first year for training and the second year for testing). As the time series of the training and test datasets in the input to the classifiers must have the same number of S1 images, and considering the different number of S1 images in the different datasets, it is imperative to match the number of S1 images in the training and test datasets. In cases where the number of S1 images differed, some images were removed from the larger

dataset. Firstly, we eliminated one image per month from the larger dataset, starting with the first months of the S1 time series. Next, this process was repeated until the sizes of the two datasets were harmonized. For example, for the combination where the training year was 2018 and the test year was 2019, the training dataset comprised 121 images while the test dataset had 110 images for window 3. In this case, 11 images needed to be removed from the training dataset. Consequently, two images were removed from the first 3 months and only one image from the next 5 months (the duration of W3 is 8 months).

With the aim of assessing the results of the classification procedure, we used various evaluation metrics. These metrics are recall (Equation (1)), precision (Equation (2)), F1 score (Equation (3)) for rapeseed class, and Kappa (Equation (4)):

1. Recall represents the proportion of correctly detected rapeseed (TP) compared to the total number of rapeseed fields, including also the non-detected ones (false negatives, NG) [24].
2. Precision refers to the ratio of accurately estimated rapeseed (true positives, TP) to the sum of true positives and false positives (instances that were incorrectly predicted as positive) [24].
3. F1 score is defined as the harmonic mean of precision and recall measurements [24]. The F1 score is a metric that combines precision and recall into a single value, providing a balance between these two measures. The F1 score ranges from 0 to 1, where 1 indicates perfect precision and recall, and 0 indicates poor performance in either precision or recall. However, we presented it on a scale of percentages between 0 and 100%.
4. Kappa is a measure of the agreement between the frequencies of two sets of data collected on separate occasions. It includes both observed and expected agreement and provides a standardized assessment that accounts for chance. It is often used to assess the reliability of ratings, classifications, or observations made by different raters or methods during two different data collection sessions [25].

$$\text{Recall} = \frac{\text{TP}}{\text{TP} + \text{FN}} \quad (1)$$

$$\text{Precision} = \frac{\text{TP}}{\text{TP} + \text{FP}} \quad (2)$$

$$\text{F1} = \frac{2 * (\text{Precision} * \text{Recall})}{\text{Precision} + \text{Recall}} \quad (3)$$

$$\text{Kappa} = \frac{\text{Po} - \text{Pe}}{1 - \text{pe}} \quad (4)$$

In the context of these equations, the variables are defined as follows:

True positives (TP): The number of instances correctly predicted as positive by the model.

False positives (FP): The number of instances incorrectly predicted as positive by the model.

False negatives (FN): The number of instances incorrectly predicted as negative by the model.

Observed agreement (Po): The proportion of agreement between two raters or methods based on the actual observed data. It is calculated as the sum of true positives and true negatives divided by the total number of instances [26].

Expected agreement (Pe): The expected agreement that occurs by chance. It is calculated based on the marginal probabilities of agreement for positive and negative instances [26].

3. Results

3.1. Sentinel-1 Backscattering Analysis

Figure 2 illustrates the temporal behavior of the S1 backscattering coefficient (σ°) for rapeseed fields in our study area over three rapeseed cultivation years: 2018, 2019, and 2020. The rapeseed cultivation season in La Rochelle starts from late August to early September and ends between late June and early July each year. During the sowing period at our study site (September to November), the S1 backscattering coefficient increased significantly, indicating the emergence of the plants and the development of their first leaves. Specifically, the σ° -values increased from -21 to -16 dB in VH and from -13 to -8 dB in VV. This increase in S1 backscatter is associated with the growth of biomass and rapeseed plant structural changes [11,27]. Subsequently, from November to March, which is the period of the low-growth phase during winter, the values for both polarizations remained relatively stable. During the flowering phase in April and early May, the S1 signal in VV was significantly affected, with a decrease of about 2 dB, while VH remained relatively unaffected. This decrease is consistent with the results of previous studies [10,13]. According to the findings of El Hajj et al. [28], which showed that the level of S1 stability is better than 0.48 dB (standard deviation of σ°), a change in the radar signal of more than 1 dB is considered significant. Therefore, the observed decrease of about 2 dB in the VV polarization during the flowering phase is considered significant, exceeding the 1 dB threshold (approximately twice the standard deviation) and indicating a substantial change in the radar signal associated with this growth stage. After flowering, both polarizations gradually increased, reaching a peak in May–June (approximately -11 dB in VH and -8 dB in VV), which is the period of stem elongation, inflorescence emergence, and fruit development. However, Figure 2 shows that there is a shift of up to about 2 weeks between the years in the position of the characteristic rapeseed peak (date). After this peak, both polarizations gradually decreased and returned to values similar to those at the beginning of the cycle in September. The characteristic shape exhibited by the S1 time series in accordance with the rapeseed’s phenological cycle, represents a significant advantage for mapping rapeseed fields. Consequently, approaches such as DL algorithms, leveraging end-to-end learning from input data, can capitalize on these discernible S1 signal patterns to differentiate rapeseed fields effectively. It is worth noting that VH has a more pronounced dynamic throughout the rapeseed phenological cycle compared to VV, making it indispensable for rapeseed mapping.

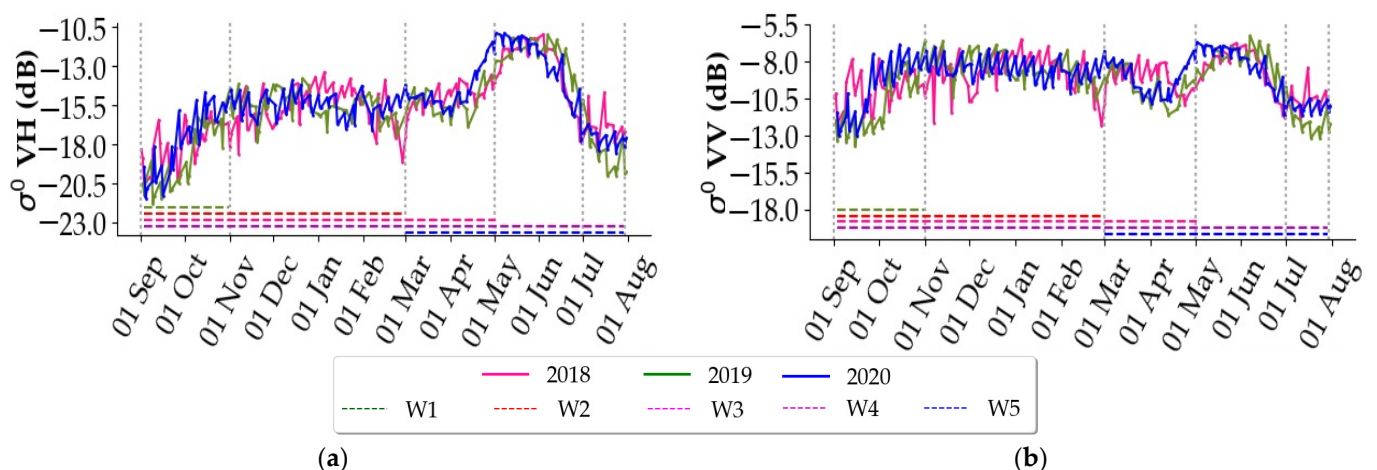


Figure 2. Time series of S1 average backscattering coefficients (σ°) for rapeseed fields in La Rochelle for each year (2018, 2019, and 2020). (a) VH and (b) VV polarizations. The five temporal windows used to examine the effect of the S1 observation window on the accuracy of rapeseed classification are represented by dashed lines (W1 = window 1; W2 = window 2; W3 = window 3; W4 = window 4; W5 = window 5).

Based on the biophysical variation of rapeseed in the S1 time series, we adopted five time windows in this study, which are represented by the dashed lines in Figure 2. The first window spans from September to November, covering the sowing period at our study site. Our second temporal window, from September to March, included significant signal increases during both plant emergence and the low-growth phase. The third temporal window, from September to early May, captured the flowering and preceding phases. The fourth temporal window covered the whole rapeseed growth cycle (1 September–1 August). The fifth temporal window focused on the peak period of the signals corresponding to the period of stem elongation, inflorescence emergence, and fruit development (1 March–1 August).

3.2. Effective Temporal Windows for Rapeseed Mapping

To assess the potential for early-season rapeseed detection and the classification performance when only utilizing part of the S1 time series (only a part of the growth cycle), classification by RF and InceptionTime was performed in two scenarios, including the same year as the training and test and different years to the train and test (temporal transferability of the classifier). The performance of both methods in each scenario was evaluated using F1, precision, recall per rapeseed class, and Kappa coefficient metrics.

3.2.1. Effective Temporal Windows for Rapeseed Detection in the Same Year

In this section, classification was performed over five temporal windows, covering various phases of the rapeseed phenological cycle at the La Rochelle study site. Detailed descriptions of these windows can be found in Section 3.1 (Figure 2). This evaluation uses S1-VV and S1-VH data from the same year for training and testing (2018, 2019, and 2020) to determine the performance of rapeseed detection in each temporal window.

The outcomes of the performance assessment for rapeseed classification are represented in Table 2, considering the F1 score, precision, recall, and Kappa coefficient. The highest F1 score and Kappa are attained when employing three temporal windows: 1 September–1 May (W3: an 8-month time series), 1 September–1 August (W4: an 11-month time series), and 1 March–1 August (W5: a 5-month time series). The InceptionTime method provided F1 values of 95.3%, 96.1%, and 96.2%, along with Kappa values of 0.95, 0.96, and 0.96, respectively, using W3, W4, and W5. RF gave F1 scores of 92.2%, 95.1%, and 95.1%, coupled with Kappa values of 0.92, 0.95, and 0.95, respectively, for the same set of windows. Therefore, both algorithms provide high accuracy for rapeseed field detection using W3, W4, or W5. In addition, the results revealed precision and recall rates above 90% when using these three temporal windows. Notably, applying W5 enables the approaches to achieve high accuracy with a smaller volume of S1 data. The feature importance analysis using RF, as shown in Figure 3, further confirms the importance of this period for rapeseed detection. In particular, the main rapeseed growth period between April and June, especially in May, which contains the peak S1 backscatter, has the highest importance for rapeseed detection using RF in all three years of the study. This confirms that our results, which were based on considering different growth stages, align with a statistical analysis that measures the importance of variables.

In the case of the other two windows, specifically W1 (1 September–1 November) and W2 (1 September–1 March), InceptionTime and RF provide lower accuracies. These two windows correspond to the S1 time series, which covers the first part of the rapeseed growth cycle before reaching the flowering period. The W1 and W2 time series commence at sowing and end two months and 6 months later, respectively. Inception Time yielded F1 values of 77.2% and 89.0%, along with a Kappa of 0.77 and 0.89, respectively, for W1 and W2. While RF produced F1 values of 67.5% and 80.0%, with corresponding Kappa values of 0.67 and 0.79, respectively, for W1 and W2, the lower recall value is the reason for the lower F1 scores using these windows (recall values of 54.5% and 68.7% by RF, 74.3% and 85.9% by InceptionTime, for W1 and W2, respectively). The results of this analysis indicate that when the training and test data are from the same

year, rapeseed can be detected with moderate accuracy before flowering with both RF and InceptionTime.

Table 2. The results of the accuracy assessment for classification using the same-year training and test datasets with the selected five temporal windows of the rapeseed growth cycle. “Mean” represents the average value across all three years. “Max” and “Min” correspond to the highest and lowest values observed within the three years, respectively. The bold values indicate the highest performance.

| Temporal Window | Classifier | F1 (%) | | | Precision (%) | | | Recall (%) | | | Kappa | | |
|-----------------|------------|-------------|-------------|-------------|---------------|-------------|-------------|-------------|-------------|-------------|-------------|-------------|-------------|
| | | Mean | Min | Max | Mean | Min | Max | Mean | Min | Max | Mean | Min | Max |
| W1 | RF | 67.5 | 55.5 | 78.6 | 92.6 | 90.0 | 96.8 | 54.5 | 39.0 | 69.7 | 0.67 | 0.55 | 0.78 |
| | Inception | 77.2 | 72.3 | 84.3 | 80.9 | 74.8 | 86.9 | 74.3 | 70.3 | 82.0 | 0.77 | 0.72 | 0.84 |
| W2 | RF | 79.8 | 75.9 | 86.0 | 95.7 | 94.9 | 97.4 | 68.7 | 63.3 | 78.5 | 0.79 | 0.76 | 0.86 |
| | Inception | 88.9 | 87.2 | 91.1 | 92.3 | 90.9 | 94.5 | 85.9 | 83.1 | 90.7 | 0.89 | 0.87 | 0.91 |
| W3 | RF | 92.2 | 89.9 | 93.7 | 97.6 | 96.8 | 98.0 | 87.5 | 83.9 | 89.8 | 0.92 | 0.90 | 0.94 |
| | Inception | 95.3 | 94.6 | 95.8 | 95.8 | 95.6 | 96.0 | 94.8 | 93.3 | 96.0 | 0.95 | 0.94 | 0.96 |
| W4 | RF | 95.1 | 94.2 | 95.7 | 97.4 | 97.3 | 97.7 | 92.9 | 91.4 | 93.8 | 0.95 | 0.94 | 0.96 |
| | Inception | 96.1 | 95.9 | 96.5 | 95.7 | 95.5 | 96.0 | 96.5 | 96.3 | 97.0 | 0.96 | 0.96 | 0.96 |
| W5 | RF | 95.1 | 94.4 | 95.9 | 97.5 | 97.4 | 97.5 | 92.9 | 91.6 | 94.5 | 0.95 | 0.94 | 0.96 |
| | Inception | 96.2 | 95.6 | 96.5 | 96.1 | 95.9 | 96.3 | 96.3 | 95.4 | 96.8 | 0.96 | 0.96 | 0.97 |

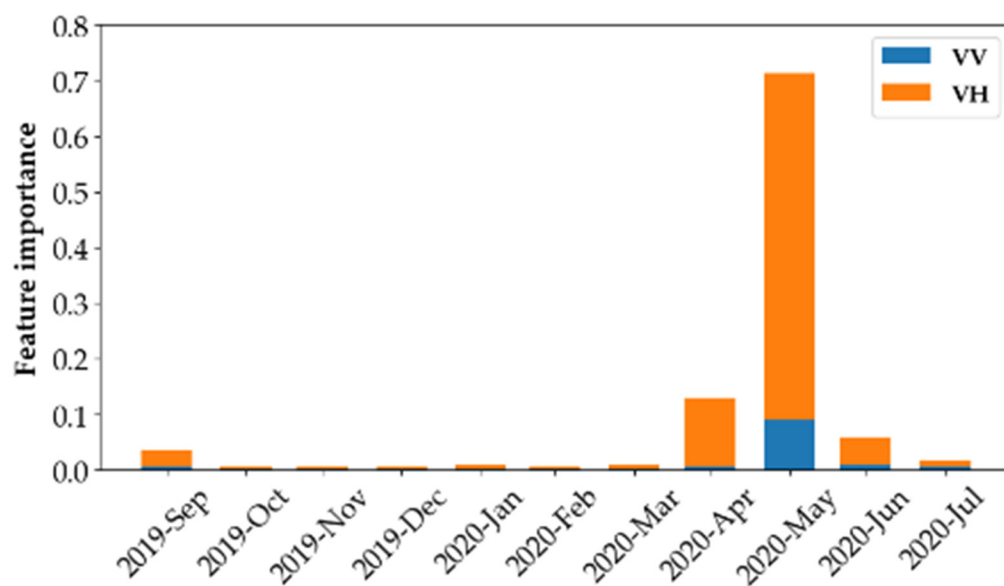


Figure 3. RF feature (dates) importance grouped per month when the same year was used for both training and testing (2020). The entire S1 time series was used (W4). Similar findings are obtained using other years.

A regression analysis conducted on the relationship between the number of S1 images and the F1 score for rapeseed classification across five temporal windows, using the same year for both training and test datasets (as depicted in Figure 4a,b for RF and InceptionTime, respectively), yielded R-squared values of 0.48 and 0.53 for the RF and InceptionTime algorithms, respectively. These results suggest that only a portion of the variability in accuracy data can be attributed to the number of S1 images. However, it is evident that other factors, such as the characteristic shape of the S1 backscatter during the main rapeseed growth cycle, also influence achieving a high F1 score within a short time series (W5). Such a shape facilitates the detection of rapeseed, as this shape does not appear in the S1 backscatter of other main crops in the study area, especially in the VH polarization (Figure 5). Furthermore, it is noteworthy that the choice of algorithm—RF or

InceptionTime—plays a major role, with InceptionTime demonstrating a slightly superior ability to explain the variability in accuracy based on the number of S1 images.

The rapeseed map derived from the training and test data belonging to the same year using W2 and W5 windows within a specific section of the study area (Figure 6a) is presented by Figure 6b–e, which involves early rapeseed detection and achieving high accuracy with a short time series. In Figure 6b, it is evident that InceptionTime, when applied with window 2 (W2), accurately classified rapeseed, underscoring the algorithm’s capability for early rapeseed detection. However, with the same window, RF exhibited a higher number of misclassifications, wrongly identifying some rapeseed classes as non-rapeseed (Figure 6c). Regarding the use of window 5 (W5) for rapeseed detection, Figure 6d,e show the output of the InceptionTime and RF algorithms, respectively. Both algorithms successfully produced accurate rapeseed maps using a reduced number of images. However, some misclassifications still exist, and they concern small rapeseed fields. This can probably be related to the spatial resolution of 10 m associated with the S1 images.

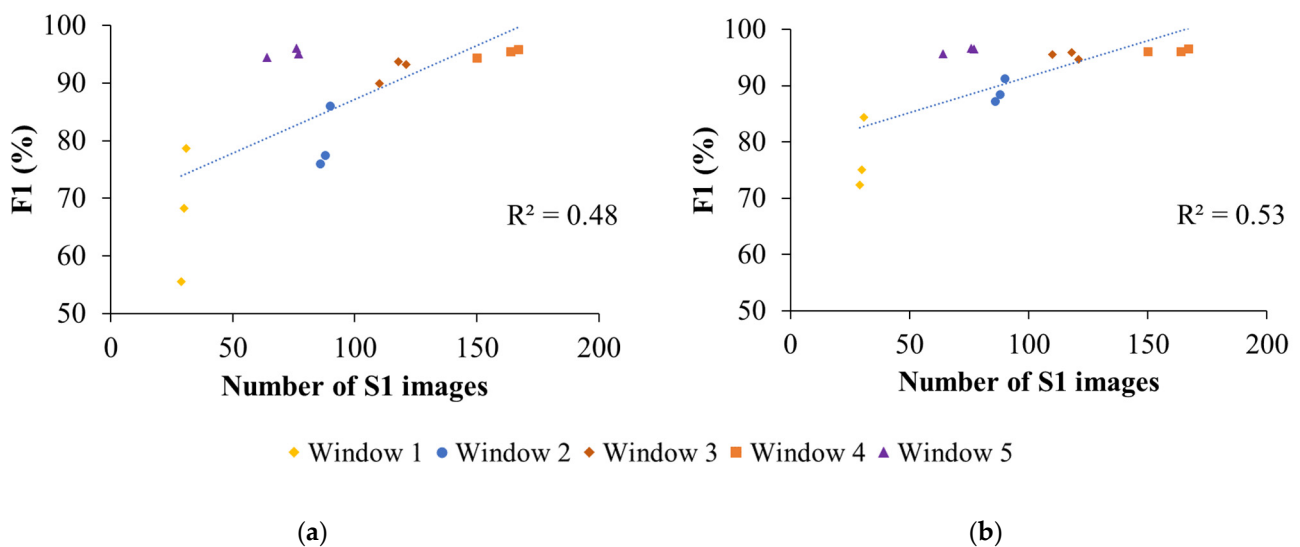


Figure 4. The regression analysis between the number of S1 images and the F1 score of rapeseed classification with the same year for training and testing using (a) RF and (b) InceptionTime. Five temporal windows are represented (W1, W2, W3, W4, and W5).

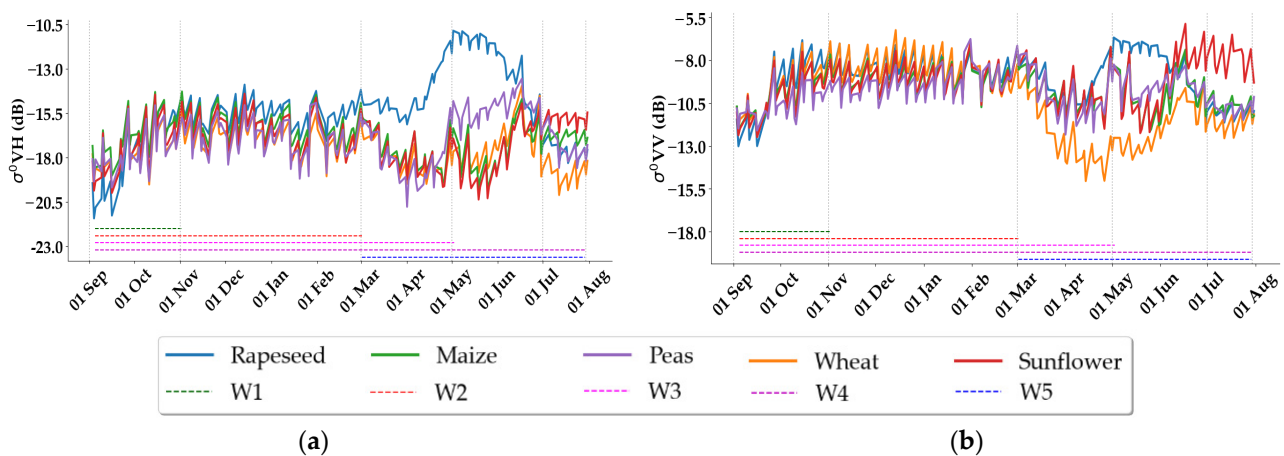


Figure 5. Time series of S1 average backscattering coefficients (σ°) for five main crop types in our study site. (a) VH, and (b) VV polarizations. Our five temporal windows are represented by dashed lines (W1 = window 1; W2 = window 2; W3 = window 3; W4 = window 4; W5 = window 5).

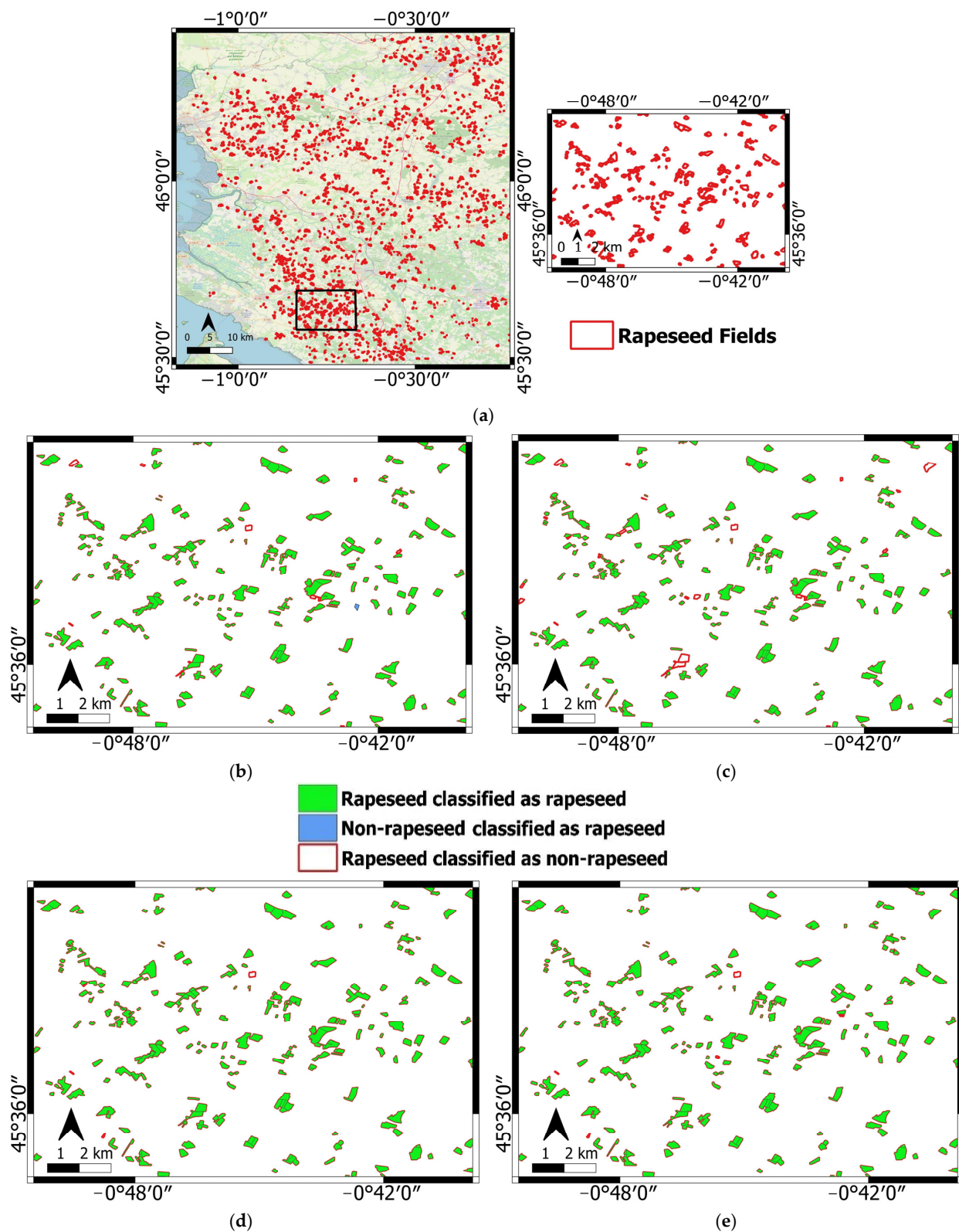


Figure 6. Rapeseed maps of La Rochelle in 2020 generated from the S1 time series of the same year for training and testing, using the windows W2 and W5 within a specific section of the study area (a): (b) W2 using the InceptionTime algorithm, (c) W2 using the RF algorithm, (d) W5 using the InceptionTime algorithm, and (e) W5 using the RF algorithm. Rapeseed fields correctly classified as rapeseed are shown in green; non-rapeseed fields classified as rapeseed are in blue; and rapeseed fields classified as non-rapeseed are shown with a polygon outline in red.

3.2.2. Effective Temporal Windows for Rapeseed Detection Using the Different Years as Training and Test

In this section, we evaluate the effect of the temporal window on rapeseed detection using different years as training and test datasets. We classified three temporal windows of the S1 time series: W2 to evaluate temporal transferability in early rapeseed detection; W5 to investigate transferability within a short time series; and W4, representing the time series covering the entire rapeseed growth cycle. For early rapeseed detection, we chose W2 over W1 and W3 based on the results of the previous scenario. Although W3 outperformed two other windows, W2 was used in classification because it gave a good F1 result while using a shorter temporal window.

Table 3 shows the classification results using RF and InceptionTime over three different windows. As shown in Table 3, the RF and InceptionTime algorithms yielded mean F1 values of 45.6% and 41.0%, respectively, when using W2. Consequently, it proved challenging to produce an accurate early rapeseed map for one year using another year's training data. The main factor contributing to these suboptimal results was the low recall observed for both algorithms, which was 34.3% for RF and 33.2% for InceptionTime. This low recall indicates that a limited number of rapeseed fields were correctly detected. In terms of precision, RF achieved a better performance (85.9%) than InceptionTime (74.8%) with W2. In contrast, the use of W5, corresponding to the S1 time series around the main peak of rapeseed, resulted in substantially higher mean F1 scores of 92.0% and 90.0% for RF and InceptionTime, respectively. These results are very similar to the ones obtained with the full rapeseed growth cycle (W4). Therefore, W5 seems to represent the most efficient option, as it requires a reduced number of image acquisitions compared to the full time series (W4). The results of feature importance using RF for the combinations of the training and test years with the lowest (Figure 7a), and the highest F1 scores (Figure 7b), further confirm the significance of this time window for detecting rapeseed fields when utilizing different years for training and tests. Notably, the main growth period of rapeseed from April to June, particularly in May with its high S1 backscatter, ranked highest in terms of importance for rapeseed detection using RF. Figure 7 illustrates the consistency of our findings based on windows aligned with growth cycles and a statistical study assessing variable importance.

Table 3. The results of the accuracy assessment for classification using different years for training and test. The three temporal windows of rapeseed growth cycle (W2, W4, and W5) were investigated. “Mean” represents the average value across all combinations of years. “Max” and “Min” correspond to the highest and lowest values observed within all combinations of years, respectively. The bold values indicate the highest performance.

| Temporal Window | Classifier | F1 (%) | | | Precision (%) | | | Recall (%) | | | Kappa | | |
|-----------------|------------|-------------|-------------|-------------|---------------|-------------|-------------|-------------|-------------|-------------|-------------|-------------|-------------|
| | | Mean | Min | Max | Mean | Min | Max | Mean | Min | Max | Mean | Min | Max |
| W2 | RF | 45.6 | 16.3 | 64.8 | 85.9 | 70.6 | 99.0 | 34.3 | 8.9 | 53.7 | 0.45 | 0.16 | 0.65 |
| | Inception | 41.0 | 23.7 | 57.9 | 74.8 | 43.6 | 95.9 | 33.2 | 13.6 | 58.8 | 0.40 | 0.23 | 0.57 |
| W4 | RF | 92.6 | 87.8 | 95.7 | 96.6 | 94.6 | 98.6 | 89.3 | 79.1 | 96.1 | 0.92 | 0.88 | 0.96 |
| | Inception | 92.2 | 89.9 | 93.7 | 97.6 | 96.8 | 98.0 | 87.5 | 83.9 | 89.8 | 0.92 | 0.90 | 0.94 |
| W5 | RF | 92.0 | 88.3 | 94.9 | 95.2 | 91.1 | 98.6 | 89.2 | 79.8 | 96.4 | 0.92 | 0.88 | 0.95 |
| | Inception | 90.0 | 78.3 | 93.4 | 98.1 | 97.2 | 99.3 | 83.4 | 64.7 | 90.0 | 0.90 | 0.78 | 0.93 |

The regression analysis between the number of S1 images and F1 scores for rapeseed classification across the three chosen temporal windows (W2, W4, and W5), assessing temporal transferability, is illustrated in Figure 8a for RF and Figure 8b for InceptionTime, respectively. R-squared values lower than 0.1 suggest that the variability in the accuracy data cannot be explained by the number of S1 images.

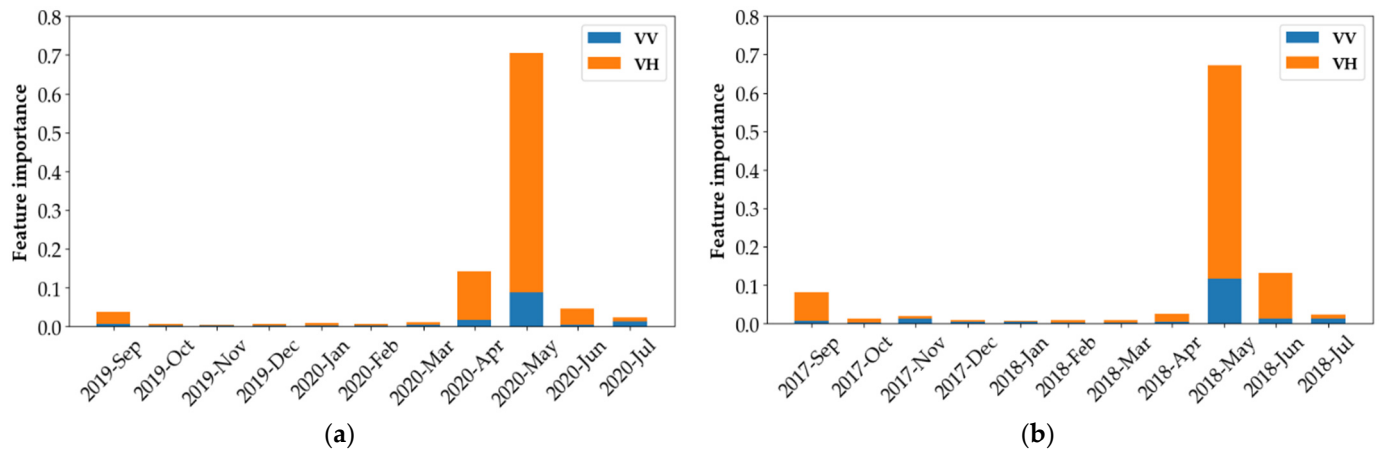


Figure 7. RF feature importance when different years were used for training and testing using the W4 time series. (a) The combination of training (2020) and test (2018) years with the lowest F1 score (81.4%); (b) the combination of training (2018) and test (2019) years with the highest F1 score (94.7%).

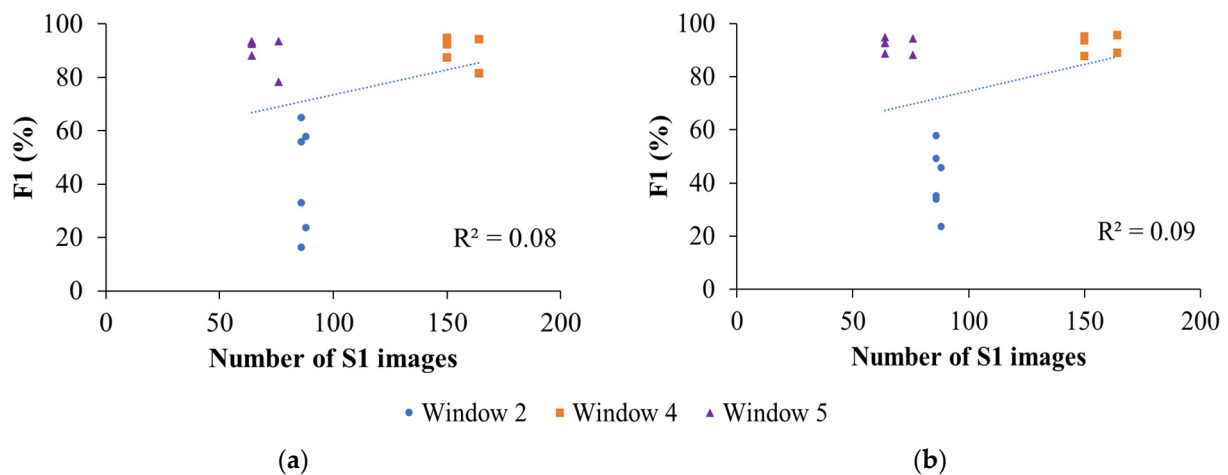


Figure 8. The regression analysis between the number of S1 images and the F1 score of rapeseed classification with different years of training and testing using (a) RF and (b) InceptionTime. Three temporal windows are represented (W2, W4, and W5).

The rapeseed maps generated for 2020 within the specific section of the study area (Figure 6a) with W2 for early rapeseed detection, using the training data of 2018, are shown in Figure 9a for InceptionTime and Figure 9b for RF. Both figures show that a significant number of rapeseed fields are misclassified as non-rapeseed by both algorithms. This is consistent with the findings in Table 3 and confirms that applying different years for training and testing does not result in an accurate map for early rapeseed detection. Notably, misclassification occurs across different sizes of rapeseed fields, which suggests that the poor results are not solely due to the spatial resolution of the images.

The rapeseed map using W5 for a short time series in the context of temporal transferability is presented in Figure 9c using InceptionTime and Figure 9d using RF (2020 for training and 2018 for testing). These figures show that both algorithms accurately detected rapeseed fields, demonstrating the feasibility of detecting rapeseed fields using the 5-month S1 time series, which aligns with the main stages of the growth cycle, encompassing stem elongation, inflorescence emergence, and fruit development. Cases of misclassification on these maps are generally confined to smaller fields, reflecting the effect of S1 spatial resolution. A comparison between maps generated with W2 (containing 6 months of images in the early stages of the growth cycle) and W5 suggests that the phenology of

rapeseed, rather than the number of images in the time series, is the more significant factor for the temporal transferability of classifiers when detecting rapeseed fields.

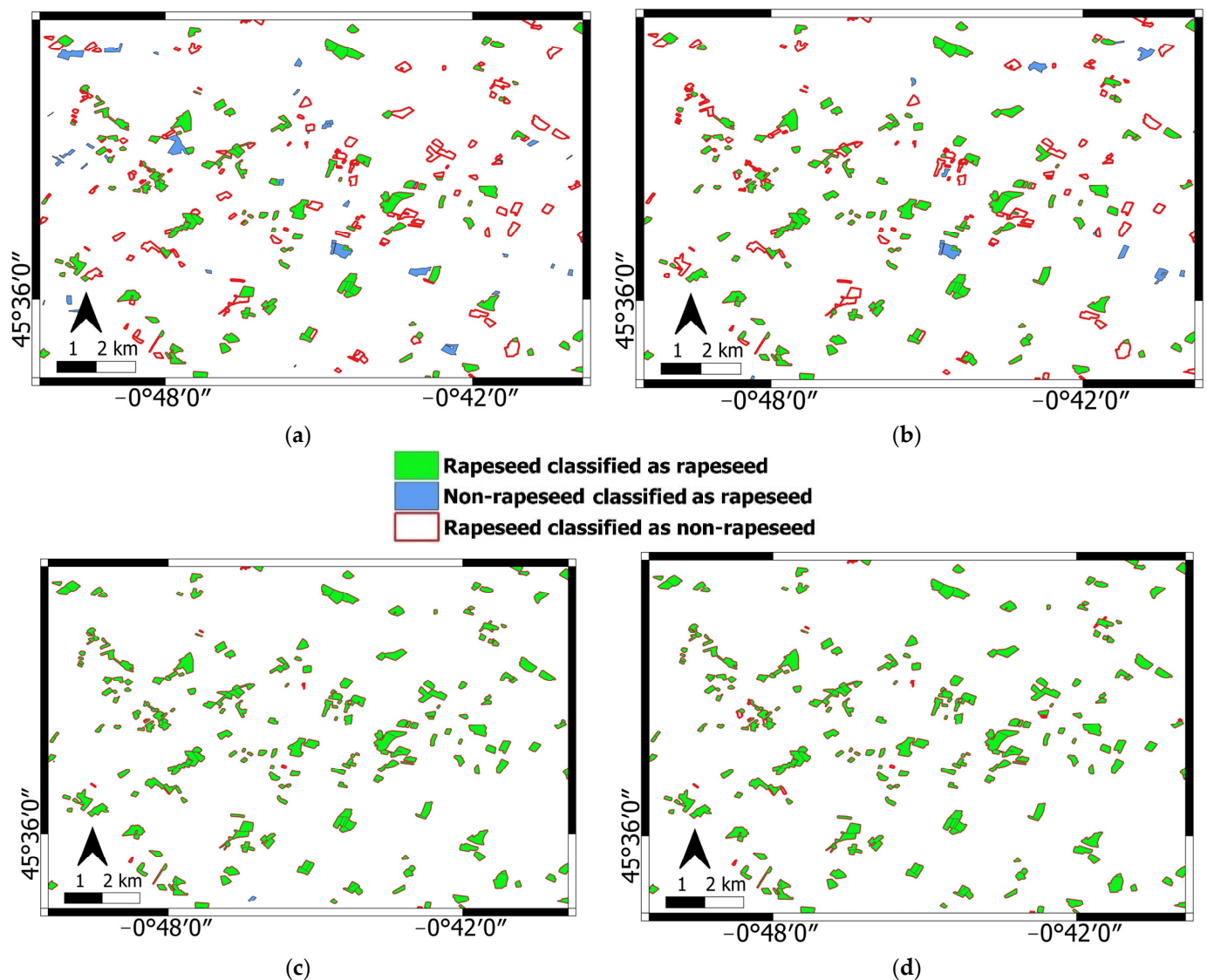


Figure 9. Rapeseed maps of La Rochelle in 2020 generated from the S1 time series of 2018 as training data, using the windows W2 and W5 within the specific section of the study area presented in Figure 6a: (a) W2 using the InceptionTime algorithm, (b) W2 using the RF algorithm, (c) W5 using the InceptionTime algorithm, and (d) W5 using the RF algorithm. Rapeseed fields correctly classified as rapeseed are shown in green, non-rapeseed fields classified as rapeseed are in blue, and rapeseed fields classified as non-rapeseed are shown with a polygon outline in red.

4. Discussion

This study focused on evaluating the impact of S1 time series size on rapeseed detection, with a specific emphasis on early detection and achieving high accuracy even using smaller time series. Efficiently mapping rapeseed fields by utilizing a reduced portion of the S1 time series leads to a decrease in processing time, involving fewer images to download, simplified image preprocessing, and accelerated algorithm execution for mapping [1,17]. It is worth noting that more data does not always equate to better performance, as demonstrated by previous studies [2]. Sometimes, an increase in data can even result in decreased accuracy, which is known as the Hughes effect [29]. In the context of crop detection studies, not every image from every time period provides valuable information for classification [2].

Moreover, decisionmakers and stakeholders in crop mapping often require early crop identification [16,30]. To address these concerns about the effective temporal window for rapeseed detection, we conducted an accuracy assessment analysis focusing on various temporal windows, spanning different phases of the rapeseed phenological cycle. This analysis aimed to determine the most effective periods for rapeseed field detection. The classification was performed in two scenarios: using the same year as training and testing across five temporal windows, and applying different years as training and testing over three temporal windows.

4.1. Effective Temporal Windows in the Same Year as Training and Testing

In the first scenario that used the same year as training and testing, which is consistent with prior research [31–33], our study revealed an improvement in the classification performance over time. As depicted in Table 2, when employing the same year for training and testing, both our algorithms, RF and InceptionTime, consistently yielded the highest F1 score and Kappa coefficient values in three temporal windows. These windows include W3, spanning from the beginning of the rapeseed growth cycle to rapid spring growth and flowering; W4, covering the entire growth stage of rapeseed; and W5, including stages of stem elongation, inflorescence emergence, and fruit development. Both considered algorithms, InceptionTime and RF, achieved F1 scores around 95% and Kappa values close to 0.95 in these three temporal windows. Meng et al. [2] also demonstrated that the Sentinel-1 time series data from the later stages of rapeseed growth in Zhongxiang, China, exhibited higher accuracy compared to early-stage time series.

In addition to the F1 score and Kappa coefficient, precision and recall are vital metrics for assessing classification algorithm performance. The results indicated that, when utilizing temporal windows W3, W4, or W5, both InceptionTime and RF consistently achieve precision and recall rates above 90%. High precision implies that when the algorithms classify an area as a rapeseed field, it is highly likely to be accurate. High recall values suggest that the algorithms can effectively detect a large proportion of the actual rapeseed fields within these temporal windows. These findings suggest that both algorithms are effective in detecting rapeseed fields during the later stages of the growth cycle, particularly during the flowering and maturation phases. Our study highlights that the use of W5 provides high accuracy in the detection of rapeseed fields while using a reduced amount of S1 data. In window 5, the dominant peak in the S1 time series corresponds to the rapeseed growth peak. This characteristic peak of rapeseed overlaps only very partially with the other dominant peaks of the other crops in the study area, particularly in the VH polarization (Figure 5). In fact, the shape and amplitude of the radar signal for rapeseed in VH are very different from those for other crops.

Achieving high accuracy using a short time series has practical implications, suggesting that precise results can be obtained with both RF as a decision tree ensemble algorithm and InceptionTime as a neural network algorithm, which can be advantageous in terms of data storage and processing efficiency.

Furthermore, the study explored the performance of InceptionTime and RF in two earlier temporal windows corresponding to the initial phases of the rapeseed growth cycle, W1 (encompassing the leaf production phase of rapeseed) and W2 (encompassing both the leaf production phase of rapeseed and its low-rate growth stage during winter). In these cases, results indicated a decrease in accuracy, with lower F1 scores and Kappa coefficients for both algorithms. This is attributed to lower recall values in W1 and W2, signifying a significant proportion of rapeseed fields not being detected during these earlier growth stages. However, these analyses reveal that rapeseed can be detected with moderate accuracy before flowering (F1 values and Kappa of 77% and 0.77 using RF, and 88% and 0.88 using InceptionTime, respectively). These findings have implications for the use of S1 data and artificial intelligence algorithms in agricultural monitoring, particularly for the timely detection of crop types and growth stages. Understanding the optimal temporal

windows for classification can lead to more effective and resource-efficient monitoring systems for rapeseed [34].

4.2. Effective Temporal Windows with Different Years for Training and Testing

The identification of effective temporal windows for rapeseed detection utilizing different years for training and test purposes was performed across three distinct temporal windows. W2 was employed to assess early rapeseed detection, while W4 and W5 were chosen to explore the impact of the time series size on rapeseed detection. The outcomes of early rapeseed detection, employing different years for training and testing, revealed low accuracy using both RF and InceptionTime algorithms (F1 values of 45.6% and 41.0%, respectively). Consequently, when ground samples are not available for a particular year, creating an early rapeseed map using data from other years becomes infeasible. In contrast, using a short S1 time series covering the main growth cycle of rapeseed (W5: including stages of stem elongation, inflorescence emergence, and fruit development) can yield high accuracy (exceeding 90%), which closely aligns with the results from the time series that covered the entire growth cycle (W4). Therefore, W5 seems to represent the most efficient option for the temporal transferability of classifiers, as it provides high mapping accuracy while using a reduced number of image acquisitions in comparison to the use of the full time series (W4).

It is noteworthy that although the comparison of S1 backscatter between the three years of this study (Figure 2) indicates a shift of less than one month in the highest peak of S1 backscatter between 2020 and other years, the F1 score, exceeding 90%, indicates that this slight shift in S1 backscatter, resulting from the growth cycle shift, does not significantly impact classification using a short time series. This discovery aligns with the results of our previous study using a complete time series [7]. Therefore, within this range of shift between years, employing the short time series of the main growth cycle enables the creation of a rapeseed map for one year using training data collected during the main growth period from another year.

4.3. Sources of Misclassification in Rapeseed Mapping

Misclassifications in rapeseed mapping can be categorized into two groups: false positives, where non-rapeseed is incorrectly classified as rapeseed, and false negatives, where rapeseed is mistakenly labeled as non-rapeseed. We have investigated these misclassifications in the results of the temporal transferability (different years for training and testing) of both the RF and the InceptionTime, using both W2 and W5. Beyond the classification capabilities of algorithms, we investigated two possible sources contributing to false negatives. Firstly, the size of fields, linked to the S1 pixel size (10 m × 10 m), and secondly, unusual S1 backscatter in certain rapeseed fields, attributed to irregular rapeseed growth or errors in the RPG dataset (our ground data). Analyzing the size of rapeseed fields in false negatives revealed that nearly 70% of these fields in the W5 classification using InceptionTime had an area below 1 ha and, with RF, 50% had an area below 1 ha. This highlights that with W5, the primary source of misclassification comes from the size of the fields, which is related to the spatial resolution of the S1 images. For the remaining false negatives with field sizes exceeding 1 ha, we observed that the S1 backscatter in W5 did not exhibit the typical peak associated with rapeseed fields (Figure 10a). This discrepancy could be due to a growth problem in these rapeseed fields or the presence of another crop in these fields (possible but unlikely).

Exploring false negatives in the W2 classification using both our algorithms revealed that only 20% of misclassifications occurred in fields smaller than 1 ha. Interestingly, 80% of false negatives in W2 occurred in fields larger than 1 ha, indicating that field size is not the primary source of misclassification with this window. Instead, the behavior of the S1 signal during the W2 period (initial growth stage) is similar to that of other winter–spring crops.

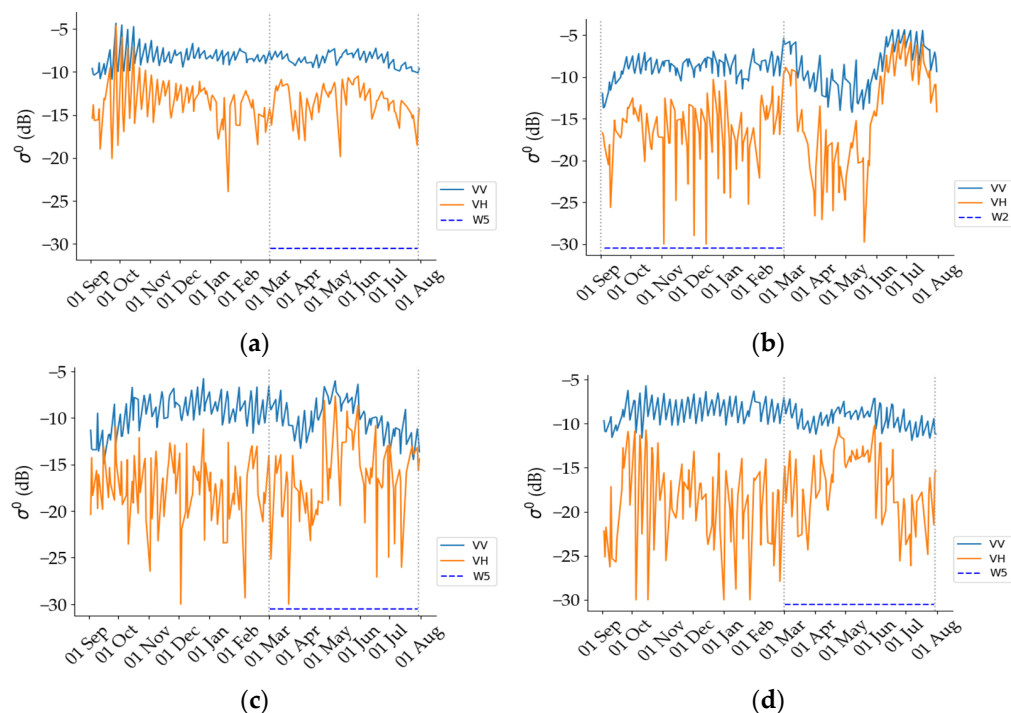


Figure 10. S1 backscatter of one false negative (a) and three false positives (b–d) from the results of classifier temporal transferability: (a) the largest rapeseed field misclassified as non-rapeseed by InceptionTime and W5 (false negative); (b) sunflower (false positive using W2); (c) fallow lands (false positive using W5); and (d) spring peas (false positive using W5).

Regarding false positives (non-rapeseed classified as rapeseed) in the W5 results, 50% of misclassifications were associated with peas and fallow lands. An examination of the S1 backscatter for peas and fallow lands during W5 (Figure 10c,d) revealed a peak similar to the rapeseed peak period, indicating the challenge of distinguishing between these classes. Using W2, 50% of misclassifications were with maize and sunflower, which have a similar S1 backscatter trend to rapeseed in this temporal window (Figure 10b for sunflower). Therefore, the main source of false positives lies in the similarity of S1 backscatter patterns between rapeseed and other crops.

5. Conclusions

In this paper, the potential for early-season rapeseed detection and the use of S1 time series only covering a part of the rapeseed growth cycle were investigated. When it comes to early-season rapeseed detection and the use of shorter time series, this study underscores the critical importance of selecting the appropriate temporal window for precise rapeseed detection. The results demonstrated that utilizing a short time series covering the main growth stages of rapeseed (W5: a 5-month time series encompasses stem elongation, inflorescence emergence, and fruit development) yielded comparable outcomes to an extended time series (W4: an 11-month time series encompasses the entire growth stage). Using both windows, our algorithms yielded mean F1 scores ranging between 95.1% and 96.2% with the same-year training and test data and between 90.0% and 92.6% using different years for training and testing. Specifically, for early rapeseed detection within a temporal window starting at sowing and extending to six months post-sowing (W2), RF and InceptionTime achieved mean F1 scores of 79.8% and 88.9%, respectively, using the same year as training and testing. However, in the scenario of temporal transferability, both classifiers exhibited F1 scores lower than 50%, emphasizing the necessity of ground measurements for each year in early rapeseed detection.

Comparing the performance of InceptionTime and RF, both algorithms demonstrated similar performance in time series size evaluation involving the entire growth cycle (W4)

and main growth cycle (W5). However, in early rapeseed detection, InceptionTime outperformed RF by achieving a 10% higher F1 score.

Regarding sources of misclassification in the scenario of temporal transferability, we identified differences between temporal windows W2 (for early rapeseed detection) and W5 (a smaller time series size). Field size played a significant role in false negatives using W5 (70% for InceptionTime and 50% for RF). In W2, the behavior of the S1 signal during the initial growth stage contributed to misclassifications due to similarities with other winter–spring crops. Additionally, for both W5 and W2, false positives were attributed to the similarity of S1 backscatter patterns between rapeseed and other crops.

Our findings on temporal transferability revealed that a slight shift of less than one month in S1 backscatter, resulting from the growth cycle shift, does not significantly impact classification. Future studies should explore the effects of shifts between different study regions. Overall, this work highlights the importance of selecting specific temporal windows, considering both growth stages and efficient data utilization. The findings have practical implications for efficient agricultural monitoring.

Author Contributions: Conceptualization, N.B.; methodology, N.B.; software, S.M. and C.F.D.; formal analysis, S.M. and C.F.D.; data curation, S.M., N.B. and S.N.; writing—original draft, S.M. and N.B.; review and editing, S.M., N.B., C.F.D., D.I., S.N. and H.B.; visualization, S.M.; supervision, N.B.; project administration, N.B. All authors have read and agreed to the published version of the manuscript.

Funding: This research was funded by the French Space Study Center (CNES, TOSCA 2023 project) and the National Research Institute for Agriculture, Food, and the Environment (INRAE).

Data Availability Statement: The data presented in this study are available on request from the corresponding author. The data are not publicly available due to privacy.

Acknowledgments: The authors would like to thank the French Space Study Center (CNES, TOSCA 2023) and the National Research Institute for Agriculture, Food, and the Environment (INRAE) for their support in carrying out this research. We are also grateful to the European Space Agency (ESA) for providing the S1 images.

Conflicts of Interest: The authors declare no conflicts of interest. H.B. was employed by the company Atos France. The remaining authors declare that the research was conducted in the absence of any commercial or financial relationships that could be construed as a potential conflict of interest.

References

- Zhang, H.; Liu, W.; Zhang, L. Seamless and Automated Rapeseed Mapping for Large Cloudy Regions Using Time-Series Optical Satellite Imagery. *ISPRS J. Photogramm. Remote Sens.* **2022**, *184*, 45–62. [\[CrossRef\]](#)
- Meng, S.; Zhong, Y.; Luo, C.; Hu, X.; Wang, X.; Huang, S. Optimal Temporal Window Selection for Winter Wheat and Rapeseed Mapping with Sentinel-2 Images: A Case Study of Zhongxiang in China. *Remote Sens.* **2020**, *12*, 226. [\[CrossRef\]](#)
- Duren, I.; Voinov, A.; Arodudu, O.; Firrisa, M.T. Where to Produce Rapeseed Biodiesel and Why? Mapping European Rapeseed Energy Efficiency. *Renew. Energy* **2015**, *74*, 49–59. [\[CrossRef\]](#)
- Liu, W.; Zhang, H. Mapping Annual 10 m Rapeseed Extent Using Multisource Data in the Yangtze River Economic Belt of China (2017–2021) on Google Earth Engine. *Int. J. Appl. Earth Obs. Geoinf.* **2023**, *117*, 103198. [\[CrossRef\]](#)
- Pan, Z.; Huang, J.; Wang, F. Multi Range Spectral Feature Fitting for Hyperspectral Imagery in Extracting Oilseed Rape Planting Area. *Int. J. Appl. Earth Obs. Geoinf.* **2013**, *25*, 21–29. [\[CrossRef\]](#)
- Tao, J.; Liu, W.; Tan, W.; Kong, X.; Xu, M. Fusing Multi-Source Data to Map Spatio-Temporal Dynamics of Winter Rape on the Jiangnan Plain and Dongting Lake Plain, China. *J. Integr. Agric.* **2019**, *18*, 2393–2407. [\[CrossRef\]](#)
- Maleki, S.; Baghdadi, N.; Dantas, C.F.; Najem, S.; Bazzi, H.; Reluy, N.P.; Ienco, D.; Zribi, M. Artificial Intelligence Algorithms for Rapeseed Fields Mapping Using Sentinel-1 Time Series: Temporal Transfer Scenario and Ground Sampling Constraints. *IEEE J. Sel. Top. Appl. Earth Obs. Remote Sens.* **2023**, *16*, 8884–8899. [\[CrossRef\]](#)
- Ashourloo, D.; Shahrabi, H.S.; Azadbakht, M.; Aghighi, H.; Nematollahi, H.; Alimohammadi, A.; Matkan, A.A. Automatic Canola Mapping Using Time Series of Sentinel 2 Images. *ISPRS J. Photogramm. Remote Sens.* **2019**, *156*, 63–76. [\[CrossRef\]](#)
- Sulik, J.J.; Long, D.S. Spectral Considerations for Modeling Yield of Canola. *Remote Sens. Environ.* **2016**, *184*, 161–174. [\[CrossRef\]](#)
- Veloso, A.; Mermoz, S.; Bouvet, A.; Le Toan, T.; Planells, M.; Dejoux, J.-F.; Ceschia, E. Understanding the Temporal Behavior of Crops Using Sentinel-1 and Sentinel-2-like Data for Agricultural Applications. *Remote Sens. Environ.* **2017**, *199*, 415–426. [\[CrossRef\]](#)

11. Mercier, A.; Betbeder, J.; Baudry, J.; Le Roux, V.; Spicher, F.; Lacoux, J.; Roger, D.; Hubert-Moy, L. Evaluation of Sentinel-1 & 2 Time Series for Predicting Wheat and Rapeseed Phenological Stages. *ISPRS J. Photogramm. Remote Sens.* **2020**, *163*, 231–256. [[CrossRef](#)]
12. Wang, D.; Fang, S.; Yang, Z.; Wang, L.; Tang, W.; Li, Y.; Tong, C. A Regional Mapping Method for Oilseed Rape Based on HSV Transformation and Spectral Features. *ISPRS Int. J. Geoinf.* **2018**, *7*, 224. [[CrossRef](#)]
13. d’Andrimont, R.; Taymans, M.; Lemoine, G.; Ceglar, A.; Yordanov, M.; van der Velde, M. Detecting Flowering Phenology in Oil Seed Rape Parcels with Sentinel-1 and -2 Time Series. *Remote Sens. Environ.* **2020**, *239*, 111660. [[CrossRef](#)]
14. Han, S.; Liu, J.; Zhou, G.; Jin, Y.; Zhang, M.; Xu, S. InceptionV3-LSTM: A Deep Learning Net for the Intelligent Prediction of Rapeseed Harvest Time. *Agronomy* **2022**, *12*, 3046. [[CrossRef](#)]
15. Waldhoff, G.; Lussem, U.; Bareth, G. Multi-Data Approach for Remote Sensing-Based Regional Crop Rotation Mapping: A Case Study for the Rur Catchment, Germany. *Int. J. Appl. Earth Obs. Geoinf.* **2017**, *61*, 55–69. [[CrossRef](#)]
16. Inglada, J.; Vincent, A.; Arias, M.; Marais-Sicre, C. Improved Early Crop Type Identification by Joint Use of High Temporal Resolution SAR And Optical Image Time Series. *Remote Sens.* **2016**, *8*, 362. [[CrossRef](#)]
17. Conrad, C.; Dech, S.; Dubovyk, O.; Fritsch, S.; Klein, D.; Löw, F.; Schorch, G.; Zeidler, J. Derivation of Temporal Windows for Accurate Crop Discrimination in Heterogeneous Croplands of Uzbekistan Using Multitemporal RapidEye Images. *Comput. Electron. Agric.* **2014**, *103*, 63–74. [[CrossRef](#)]
18. Vaudour, E.; Noirot-Cosson, P.E.; Membrive, O. Early-Season Mapping of Crops and Cultural Operations Using Very High Spatial Resolution Pléiades Images. *Int. J. Appl. Earth Obs. Geoinf.* **2015**, *42*, 128–141. [[CrossRef](#)]
19. Sujud, L.; Jaafar, H.; Haj Hassan, M.A.; Zurayk, R. Cannabis Detection from Optical and RADAR Data Fusion: A Comparative Analysis of the SMILE Machine Learning Algorithms in Google Earth Engine. *Remote Sens. Appl.* **2021**, *24*, 100639. [[CrossRef](#)]
20. Belgiu, M.; Drăguț, L. Random Forest in Remote Sensing: A Review of Applications and Future Directions. *ISPRS J. Photogramm. Remote Sens.* **2016**, *114*, 24–31. [[CrossRef](#)]
21. USDA. Oilseeds: World Markets and Trade. Feb 2023. Foreign Agricultural Service/USDA/Global Market Analysis, Washington, DC, USA, 2023. Available online: <https://fas.usda.gov/data/oilseeds-world-markets-and-trade> (accessed on 24 September 2023).
22. Rodriguez-Galiano, V.F.; Chica-Olmo, M.; Abarca-Hernandez, F.; Atkinson, P.M.; Jeganathan, C. Random Forest Classification of Mediterranean Land Cover Using Multi-Seasonal Imagery and Multi-Seasonal Texture. *Remote Sens. Environ.* **2012**, *121*, 93–107. [[CrossRef](#)]
23. Ismail Fawaz, H.; Lucas, B.; Forestier, G.; Pelletier, C.; Schmidt, D.F.; Weber, J.; Webb, G.I.; Idoumghar, L.; Muller, P.A.; Petitjean, F. InceptionTime: Finding AlexNet for Time Series Classification. *Data Min. Knowl. Discov.* **2020**, *34*, 1936–1962. [[CrossRef](#)]
24. Fränti, P.; Mariescu-Istodor, R. Soft Precision and Recall. *Pattern Recognit. Lett.* **2023**, *167*, 115–121. [[CrossRef](#)]
25. Xia, Y. Correlation and Association Analyses in Microbiome Study Integrating Multiomics in Health and Disease. In *Progress in Molecular Biology and Translational Science*; Elsevier: Amsterdam, The Netherlands, 2020; pp. 309–491.
26. Chicco, D.; Warrens, M.J.; Jurman, G. The Matthews Correlation Coefficient (MCC) Is More Informative Than Cohen’s Kappa and Brier Score in Binary Classification Assessment. *IEEE Access* **2021**, *9*, 78368–78381. [[CrossRef](#)]
27. Fieuzal, R.; Baup, F.; Marais-Sicre, C. Monitoring Wheat and Rapeseed by Using Synchronous Optical and Radar Satellite Data—From Temporal Signatures to Crop Parameters Estimation. *Adv. Remote Sens.* **2013**, *02*, 162–180. [[CrossRef](#)]
28. El Hajj, M.; Baghdadi, N.; Zribi, M.; Angelliaume, S. Analysis of Sentinel-1 Radiometric Stability and Quality for Land Surface Applications. *Remote Sens.* **2016**, *8*, 406. [[CrossRef](#)]
29. Pal, M.; Mather, P.M. Assessment of the Effectiveness of Support Vector Machines for Hyperspectral Data. *Future Gener. Comput. Syst.* **2004**, *20*, 1215–1225. [[CrossRef](#)]
30. He, Y.; Dong, J.; Liao, X.; Sun, L.; Wang, Z.; You, N.; Li, Z.; Fu, P. Examining Rice Distribution and Cropping Intensity in a Mixed Single- and Double-Cropping Region in South China Using All Available Sentinel 1/2 Images. *Int. J. Appl. Earth Obs. Geoinf.* **2021**, *101*, 102351. [[CrossRef](#)]
31. Cai, Y.; Guan, K.; Peng, J.; Wang, S.; Seifert, C.; Wardlow, B.; Li, Z. A High-Performance and in-Season Classification System of Field-Level Crop Types Using Time-Series Landsat Data and a Machine Learning Approach. *Remote Sens. Environ.* **2018**, *210*, 35–47. [[CrossRef](#)]
32. Johnson, D.M.; Mueller, R. Pre- and within-Season Crop Type Classification Trained with Archival Land Cover Information. *Remote Sens. Environ.* **2021**, *264*, 112576. [[CrossRef](#)]
33. You, N.; Dong, J. Examining Earliest Identifiable Timing of Crops Using All Available Sentinel 1/2 Imagery and Google Earth Engine. *ISPRS J. Photogramm. Remote Sens.* **2020**, *161*, 109–123. [[CrossRef](#)]
34. Lin, C.; Zhong, L.; Song, X.-P.; Dong, J.; Lobell, D.B.; Jin, Z. Early- and in-Season Crop Type Mapping without Current-Year Ground Truth: Generating Labels from Historical Information via a Topology-Based Approach. *Remote Sens. Environ.* **2022**, *274*, 112994. [[CrossRef](#)]

Disclaimer/Publisher’s Note: The statements, opinions and data contained in all publications are solely those of the individual author(s) and contributor(s) and not of MDPI and/or the editor(s). MDPI and/or the editor(s) disclaim responsibility for any injury to people or property resulting from any ideas, methods, instructions or products referred to in the content.